3D Spherical Microtissues and Microfluidic Technology for Multi-tissue Experiments and Analysis

ARTICLE *in* JOURNAL OF BIOTECHNOLOGY · JANUARY 2015

Impact Factor: 2.87 · DOI: 10.1016/j.jbiotec.2015.01.003

Journal of Biotechnology xxx (2015) xxx–xxx

Contents lists available at ScienceDirect

Journal of Biotechnology

journal homepage: www.elsevier.com/locate/jbiotec

3D spherical microtissues and microfluidic technology for multi-tissue experiments and analysis

Q1 Jin-Young Kim[a], David A. Fluri[b], Rosemarie Marchan[c], Kurt Boonen[d], Soumyaranjan Mohanty[a,1], Prateek Singh[a,2], Seddik Hammad[c,e], Bart Landuyt[d], Jan G. Hengstler[c], Jens M. Kelm[b], Andreas Hierlemann[a], Olivier Frey[a,*]

[a] ETH Zurich, Department of Biosystems Science and Engineering, Bio Engineering Laboratory, Mattenstrasse 26, 4058 Basel, Switzerland
[b] InSphero AG, Wagistrasse 27, 8952 Schlieren, Switzerland
[c] Leibniz Research Centre for Working Environment and Human Factors (IfADo), TU Dortmund University, Ardeystrasse 67, 44139 Dortmund, Germany
[d] KU Leuven, Research Group of Functional Genomics and Proteomics, Naamsestraat 59, 3000 Leuven, Belgium
[e] Department of Forensic Medicine and Veterinary Toxicology, Faculty of Veterinary Medicine, South Valley University, 83523 Qena, Egypt

ARTICLE INFO

Article history:
Received 4 September 2014
Received in revised form
20 December 2014
Accepted 5 January 2015
Available online xxx

Keywords:
Tissue engineering
"Body on a Chip"
Pro-drug activation
Cyclophosphamide
Liver
Tumor

ABSTRACT

Rational development of more physiologic in vitro models includes the design of robust and flexible 3D-microtissue-based multi-tissue devices, which allow for tissue–tissue interactions. The developed device consists of multiple microchambers interconnected by microchannels. Pre-formed spherical microtissues are loaded into the microchambers and cultured under continuous perfusion. Gravity-driven flow is generated from on-chip reservoirs through automated chip-tilting without any need for additional tubing and external pumps. This tilting concept allows for operating up to 48 devices in parallel in order to test various drug concentrations with a sufficient number of replicates. For a proof of concept, rat liver and colorectal tumor microtissues were interconnected on the chip and cultured during 8 days in the presence of the pro-drug cyclophosphamide. Cyclophosphamide has a significant impact on tumor growth but only after bio-activation by the liver. This effect was only observed in the perfused and interconnected co-cultures of different microtissue types on-chip, whereas the discontinuous transfer of supernatant via pipetting from static liver microtissues that have been treated with cyclophosphamide did not significantly affect tumor growth. The results indicate the utility and multi-tissue functionality of this platform. The importance of continuous medium circulation and tissue interaction is highlighted. Q2

1. Introduction

Q3 Cell-based assays play a key role in drug discovery and provide essential information on efficacy and toxicity of compounds already at an early stage of the developmental process. The more *in vitro* models represent tissue-specific functionality and, possibly, *in vivo* physiology, the better is the prediction of the potential impact of a drug candidate before it enters animal and clinical trials.

Two-dimensional monolayer cell culture models in multi-well microliter plates are well-established, relatively simple to apply and use, and amenable to high-throughput screening. However, cells in 2D cultures often do not reflect the morphology and functionality of their native three-dimensional phenotypes (Abbott, 2003; Ghallab, 2013; Pampaloni et al., 2007; Stewart and Marchan, 2012; Yamada and Cukierman, 2007). These limitations led to increased efforts in the last years to develop 3D cell culture models that better reproduce tissue morphology and that feature dynamic mechanical properties and a biochemical environment that resemble those of living organs (Griffith and Swartz, 2006; Hammad, 2013; Huh et al., 2011; Mazzoleni et al., 2009; Pampaloni and Stelzer, 2010; Rimann and Graf-Hausner, 2012). Besides tissues obtained from biopsies and precision-cut slices, tissue can be built from isolated or cultured cells with the aim to recreate the complex 3D structure *in vitro* to the best possible extent. Several approaches are currently pursued, which differ with respect to cell type, intended model complexity, and mechanical and biochemical cues to be applied. Many approaches are based on scaffolds that provide cells with a suitable growth environment, feature effective nutrient transport and mechanical integrity. The scaffolds include

* Corresponding author. Tel.: +41 61 387 3344; fax: +41 61 387 3994.
E-mail addresses: olivier.frey@bsse.ethz.ch, olivierfrey@me.com (O. Frey).
[1] DTU Nanotech, Department of Micro- and Nanotechnology, Technical University of Denmark, Ørsteds Plads, 2800 Kgs. Lyngby, Denmark.
[2] Biocenter Oulu, Laboratory of Developmental Biology, Faculty of Biochemistry and Molecular Medicine, University of Oulu, 90220 Oulu, Finland.

http://dx.doi.org/10.1016/j.jbiotec.2015.01.003
0168-1656/

porous substrates, such as fiber meshes and microfabricated constructs, or hydrogels, such as matrigel or alginates, where the cells are embedded into the matrix to facilitate growth (Lee et al., 2008; Ringel et al., 2005).

Spherical microtissues of various sizes can be obtained by using the hanging drop technique, in which suspended cells at specific cellular densities aggregate by gravity at the liquid air interface at the bottom of the drop. Large, scaffold-free clusters of 100–500 μm diameter have been obtained (Kelm and Fussenegger, 2004; Kelm et al., 2003; Timmins and Nielsen, 2007). Several technologies are currently available to produce such spherical microtissues that exhibit tissue-like phenotypes at large throughput with good control of the dimensions (Drewitz et al., 2011; Godoy et al., 2013; Hammad, 2013; Hsiao et al., 2012; Messner et al., 2013; Thoma et al., 2013). Spherical microtissues have been demonstrated to more closely represent *in vivo* like conditions with regard to cell morphology and functionality in comparison to 2D cell cultures (Friedrich et al., 2007; Hammad et al., 2014; Hirschhaeuser et al., 2010).

In addition to establishing suitable fabrication methods for the 3D microtissue structures, the provision of an optimal microenvironment for culturing plays a critical role (Ghafar-Zadeh et al., 2011; Powers et al., 2002). The microenvironment has to mimic *in vivo* physiological conditions including spatial and temporal dimensions and dynamics, physical interactions, and biochemical settings. Microfluidic technologies are becoming more and more interesting for cell and microtissue experiments, since cells cultured within small microfluidic structures experience realistic physiological conditions with regard to liquid-to-cell ratios, fluid residence times and the dynamics of the mechanical environment (Frimat et al., 2011, 2010; Kampe et al., 2014). Miniaturization further allows for a substantial reduction of required reagent volumes and enables precise liquid volume dosage and sampling. A number of cell-based assays in microfluidic systems have, therefore, been realized and implemented (Dittrich and Manz, 2006; El-Ali et al., 2006; Kovarik et al., 2012).

The combination of 3D tissue engineering approaches with microfluidics technology and networks also poses some challenges. In recent years, several research groups have presented different approaches. For example, cell-laden hydrogels were applied into compartments of a microfluidic network before sealing it with a cover layer (Huang et al., 2011; Sin et al., 2004). More elaborate schemes comprise several stacked layers of culturing chambers and separate fluidic layers to supply nutrients (Sung et al., 2010; Tan and Desai, 2004). Both approaches, however, require device fabrication steps that may interfere with cell culturing. Dedicated microstructures to form 3D tissue directly in the microfluidic chip have been presented by (Khademhosseini et al., 2006; Leclerc et al., 2003). They include cell-trapping structures to promote cell aggregation and spheroid formation (Hsiao et al., 2009; Jin et al., 2011; Kim et al., 2012; Ruppen et al., 2014; Torisawa et al., 2007; Wu et al., 2008), or larger compartments into which cells are loaded. The cells then form 3D tissues, which are brought into contact with perfusion through a micro post barrier that simulates endothelium (Lee et al., 2007; Toh et al., 2009; Zhang et al., 2009). Other groups performed matrix gelation or polymerization inside the chip by precisely controlling the temperature and by using laminar flow and hydrodynamic focusing (Frisk et al., 2005; Kim et al., 2007), or by assembling cell-laden hydrogels directly in the chip (Kachouie et al., 2010).

Integration of 3D tissue structures into microfluidic systems of increasing complexity may entail limited reproducibility and, therefore, larger variation of tissue responses in compound testing. This aspect becomes even more important when different 3D tissue types are to be handled in the same device and are interacting through the same circulating liquid phase. Reproducibility and predictability of cell or tissue behavior in complex experimental scenarios is a pivotal issue in all current initiatives towards more biomimetic *in vitro* models, including multi-organ devices or so-called "body-on-a-chip" configurations (Esch et al., 2014, 2011; Huh et al., 2011; Imura et al., 2010; Sung and Shuler, 2009; Wagner et al., 2013; Zhang et al., 2009). Any chosen technological approach will be a trade-off between complexity and *in vivo* resemblance on the one hand, and ease of use, reproducibility, and potential for parallelization on the other hand (Van Midwoud et al., 2011).

The main goal of the concept presented here included the development of a versatile and robust platform that combines the use of scaffold-free 3D multi-cellular spheroids with microfluidic techniques. Spheroids were reliably and flexibly produced in dedicated off-chip automated systems. We then transferred them into the microfluidic chip and positioned them reliably in micro-chambers of a liquid network with the help of gravity. An automated setup, compatible with conventional CO_2-incubators, controlled continuous gravity-driven perfusion and allowed for operating up to 48 devices in parallel. Primary rat liver microtissues showed improved metabolic activity at different flow rates and different available medium volumes over 8 days in culture. Several spheroids can be loaded into the same microfluidic network. As spheroids can be readily formed from different cell types and loaded into the chip system, multi-tissue arrangements can be configured in a highly flexible manner. As a proof of concept study, we investigated the pro-drug activation of cyclophosphamide, which became possible through interconnecting rat liver and colorectal tumor microtissues on the chip.

2. Materials and methods

2.1. Microfluidic chip design

The microfluidic chip consists of two identical, independent culturing units. Each unit comprises a straight perfusion channel, 4 microtissue (MT) compartments, and 4 MT loading channels (Fig. 1a). Two open medium reservoirs at both ends of the perfusion channel allow for direct access to the medium for simple liquid sampling and medium exchange during culturing. The MT compartments are located at the intersections of the loading channels and the perfusion channel (Fig. 1b). The loading channels have a height of 550 μm and a width of 600 μm, which is high enough to guide MTs (200–300 μm diameter in this study) along the channel. The lower height of the perfusion channel (100 μm) prevents that MTs are dragged away with the flow. Its width, *w*, has been varied for different flow rates. A critical point consists of the design of the compartment hosting the microtissue. Simple, fast and complete medium renewal, which ensures sufficient nutrient and oxygen supply are essential. At the same time shear stress to MT has to be minimized. The final version of the compartment is the result of a characterization of different designs using CFD simulations. The microtissue compartment has a diameter of 1 mm and the same height of 550 μm as the loading channel (inlet Fig. 1c). The liquid has access through side openings to the compartment and is guided around the MT, which enables an efficient liquid turnover in the compartment, but also obviates any flow from directly hitting the MT so that shear and drag forces on the MT are low (see also Fig. 3).

2.2. Microfluidic chip fabrication

The microfluidic chip was fabricated by using conventional soft-lithography processes. First, an SU-8 master was fabricated on a 4-inch silicon wafer by means of photolithography. 100 μm of SU-8 100 photoresist (Microchem Corp., USA) were spin-coated on the wafer and exposed by UV through a transparency mask to define the perfusion channel. Then 450 μm of SU-8 100 were

Please cite this article in press as: Kim, J.-Y., et al., 3D spherical microtissues and microfluidic technology for multi-tissue experiments and analysis. J. Biotechnol. (2015), http://dx.doi.org/10.1016/j.jbiotec.2015.01.003

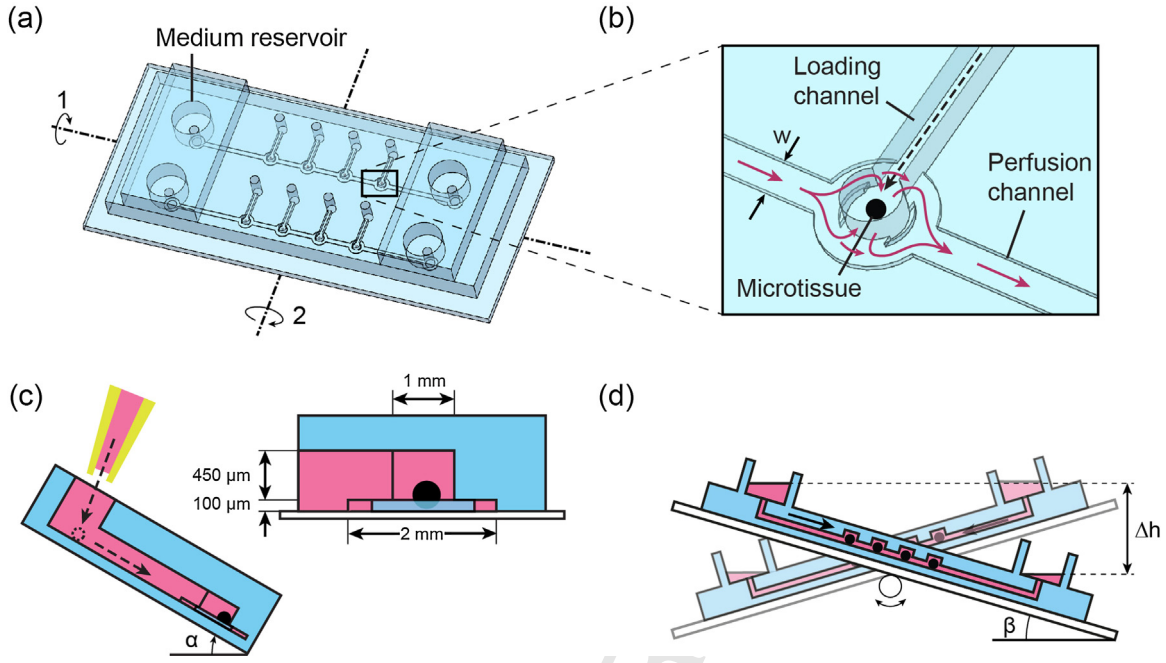

Fig. 1. (a) Schematic overview of the microfluidic chip consisting of two units; each unit comprises 4 MT compartments interconnected by a straight perfusion channel. Open medium reservoirs are located at both ends of each perfusion channel allowing for simple medium exchange. (b) Close-up of the MT compartment at the intersection of loading and perfusion channel. The black dashed arrow indicates the path of the MT during loading, the purple arrow indicates the flow in one direction (see also Fig. 3). (c) For MT loading, the chip is tilted around axis No. 1 in (a) so that gravity transfers the MT into its compartment. Dimensions of the compartment are shown in the close-up view. (d) Gravity-driven medium perfusion is achieved by periodic tilting of the chip with respect to axis No. 2 in (a).

coated on top. MT compartment and loading channels were defined by a second mask. Unexposed SU-8 was developed afterwards. Prior to use, the SU-8 master was silanized using trichloro(1,1,2,2-perfluorooctyl)silane (Sigma–Aldrich Chemie GmbH, Switzerland) in a vacuum desiccator in order to reduce PDMS adhesion.

Then, PDMS (Sylgard 184, Dow Corning, USA), mixed with its curing agent (10:1), was poured on the SU-8 master and cured at 65 °C for 4 h. The PDMS replica was then peeled off and cut into individual microchips. The PDMS channels were bonded to a glass slide (25 mm × 75 mm) after O_2-plasma treatment. Reservoirs were fabricated from PDMS and bonded to the microfluidic chip.

To prevent adsorption of cells and proteins, the PDMS channel surface was coated with Biolipidure (NOF Corp., Japan). Biolipidure contains phospholipid polar groups, 2-methacryloyloxyethyl phosphorylcholine (MPC) polymers, which are well known for the suppression of protein adsorption and denaturation on the surface (Ishihara et al., 1991). The coating solution was prepared by mixing Biolipidure, ethanol and DI water at a 1:1:3 ratio (v/v). The channel was filled with the solution and incubated for 30 min at room temperature. The channel was air-dried overnight.

2.3. CFD simulations

3-dimensional computational fluid dynamic (CFD) simulations were performed in COMSOL Multiphysics Version 3.5a (fluid dynamics model for steady-state, incompressible flow analysis) using 3D models derived from the mask designs. The microtissues were approximated by an ideal sphere with a diameter of 350 µm. Shear stresses on the sphere surface were calculated from the local fluid velocity gradients assuming no-slip conditions on the surface and dynamic viscosity for water ($\eta = 0.001$ Pa s).

2.4. Gravity-controlled microtissue loading and culturing

Gravitational forces were used to load the MTs into the chip and to culture the MTs inside the chip under continuous perfusion. Bonded and surface-treated chips were first degassed for approximately 1 hour. The chips were then sterilized under UV in a clean bench for at least 30 min; then, the channels were filled with pre-warmed-culture medium. MTs were taken up in a 200-µl-pipette tip from the GravityTRAP plate (InSphero AG, Schlieren, Switzerland) with 10 or 20 µl of medium, and released into the loading port of the loading channel. This procedure was repeated to load the required number and types of MTs into the microfluidic chip. The chip was then rotated around axis No. 1 (Fig. 1a) to a near vertical position, allowing all loaded MTs to be transferred to the respective culturing compartments at once under the influence of gravity. This ensured simultaneous and controlled loading of all MTs into the chip (Fig. 1c). The loading ports were then closed with PDMS pins.

The loaded chips were placed in a rectangular cell culture plate (Nunc OmniTray™, Milian SA, Switzerland). A PBS-soaked pad was placed around the chips to minimize evaporation of the medium. The plates were stacked on an automated tilting platform, which can be programmed with respect to tilting frequency, angle and tilting speed. The whole set-up was placed in a 5% CO_2, 37 °C humidified incubator.

Tilting the chip by a specific angle around axis No. 2 (Fig. 1a) moves the two opposed reservoirs to different heights, resulting in a flow of medium from the higher reservoir to the lower one (Fig. 1d). Complete drainage of the reservoir is prevented by capillary forces. The gravity-driven flow rate results from the height difference, Δh, of the two reservoirs:

$$\Delta h = L \cdot \sin\beta$$

for a specific tilting angle, β, and a distance, L, between the reservoirs corresponding to the microchannel length. The volumetric flow rate in the microchannel is given by

$$Q = \frac{\Delta P}{L \cdot R_f}$$

Please cite this article in press as: Kim, J.-Y., et al., 3D spherical microtissues and microfluidic technology for multi-tissue experiments and analysis. J. Biotechnol. (2015), http://dx.doi.org/10.1016/j.jbiotec.2015.01.003

with R_f being the specific resistance of the channel and ΔP the hydrostatic pressure difference given by

$$\Delta P = \rho \cdot g \cdot \Delta h$$

For calibration experiments, we tilted the platform to 30° and measured the transferred volumes after 1, 2, 3 and 5 min for different perfusion channel widths, w, (80, 600 and 800 μm). An initial volume of 50 μl of cell culture medium was used.

2.5. Cell culture

HCT116 eGFP cells (Sirion Biotech, Germany) were cultured in RPMI 1640 growth medium (Chemie Brunschwig AG, Switzerland) supplemented with 10% fetal bovine serum, 100 μg/ml penicillin, 10 μg/ml streptomycin and 0.3 μg/ml puromycin in a humidified incubator at 37 °C and 5% CO_2. The supplementary reagents were purchased from Sigma–Aldrich Chemie GmbH, Switzerland.

2.6. Microtissues

Primary rat liver microtissues (rLiMTs, initial diameter of approximately 250 μm) were provided ready to use by InSphero (InSphero AG) in GravityTRAP plates. Colorectal cancer (HCT-116 eGFP) MTs were formed in the hanging drop within 3 days with an initial number of 250 cells resulting in a MT diameter of approximately 180 μm. Medium was exchanged every 2 days for static control experiments. Six rLiMTs were pooled in 50 μl rat liver microtissue medium (InSphero AG) in a single well for static cyclophosphamide activation experiments. After a 2-day incubation period, medium was manually transferred on HCT116-eGFP composed microtissues.

2.7. Microtissue culture in the microfluidic device

Different numbers of MTs were loaded into the device, depending on the desired medium volume per MT. Four and two rLiMTs were cultured in a total volume of 25 μl to achieve conditions of 6.25 μl/MT and 12.5 μl/MT. For conditions of 40 μl/MT, only one single rLiMT was loaded in the device with 40 μl of medium. The CP bio-activation experiment included three rLiMTs in the first three MT compartments and one single HCT116 MT in the last compartment. 25 μl of medium were perfused at a flow rate of 13 μl/min. The medium was exchanged through the open reservoirs by pipetting every 2 days. Capillary forces prevent that the medium is removed from the channels (~2 μl) so that MTs always remain in liquid phase. An additional washing step may be used for complete medium renewal.

2.8. Biochemical assays

The amount of albumin in the collected supernatants was determined by using an enzyme-linked immunosorbent assay (ELISA) (Bethyl Laboratories, USA) according to manufacturer's instructions. Albumin was chosen, because it is a protein synthesized by the liver and is a well-established and specific biomarker for the metabolic activity of the liver (Ullrich et al., 2009). Reference serum standards (0–125 ng/ml for human albumin and 0–400 ng/ml for rat albumin in sample diluents) were used for the calibration curve to calculate the albumin concentration of the samples. All supernatant samples were measured in duplicates. The absorption was measured at 450 nm with a plate reader (Tecan Infinite M200 Pro, TECAN, Switzerland).

At the end of the experiments, MTs were unloaded from the chip, and a luminescence-based ATP assay (CellTiter-Glo, Promega AG, Switzerland) was conducted to determine cell viability. After the PDMS pins had been removed, MTs were automatically dragged towards the loading ports of the compartment. In case that MTs stayed in the compartment, tilting of the device (axis No. 1 in Fig. 1a) helped to transfer them back to the loading port. MTs were withdrawn with 20 μl of rLiMT maintenance medium (serum free medium) by using a conventional pipette and then transferred to an opaque 96-well plate (White half-area plate, Greiner Bio-One, Germany) for conducting the ATP assay. 5 concentrations of ATP standard solutions (0, 0.1, 0.5, 1 and 10 μM) in 20 μl of rLiMT maintenance medium were prepared in the same plate for obtaining the calibration curve. 20 μl of CellTiter-Glo reagent were added to each well, and the luminescence was measured with the plate reader.

2.9. Microscopy

The size of MTs was measured optically every 2 days using an inverted microscope (Axiovert 25, Carl Zeiss AG, Switzerland) with 5× and 10× objectives in bright-field mode. Prior to the confocal imaging, MTs were unloaded from the device for fixation. They were kept in Roti®-Histofix 4% (Carl-Roth, Karlsruhe, Germany) at 4 °C for 3 days. Subsequently, they were transferred into the second buffer, which is a mixture of Roti®-Histofix 4% and 1x PBS (1:1 v/v) containing 0.83 M of glucose. After the fixation, MT can be stored at 4 °C for up to 12 months. Immunofluorescence staining was performed on floating MTs (Hammad et al., 2014). To visualize the microarchitecture, rLiMTs were incubated with primary antibodies against DPPIV/CD26 (R&D system; AF954, 1:50) and the matching secondary antibodies. Either Cy5 conjugated anti-goat (Dianova, 1:200, Hamburg, Germany) or Alexa647 conjugated anti-goat (Dianova, 1:200, Hamburg, Germany) were used. Alexafluor 488 conjugated phalloidin (Invitrogen, 1:250) or rhodamine conjugated phalloidin (Invitrogen, 1:250) was used to label the actin cytoskeleton, and DAPI to counterstain the nuclei. HCT116 MTs were incubated with Alexafluor 488 conjugated phalloidin (Invitrogen, A12379, 1:250) to label the cytoskeletal area, as well as DAPI to counterstain the nuclei. Confocal microscopy was performed on an Olympus confocal laser microscope (FV1000, Hamburg, Germany).

2.10. Mass spectrometry

All reagents (HPLC grade) for LC-MS were purchased from Sigma Aldrich Chemie GmbH (Steinheim, Germany). Milli-Q water was prepared freshly (Millipore Corp., Bedford, USA). Supernatants for MS analysis were shock-frozen right after collection. A volume of 15 μl was transferred in a v-bottom cryotube and frozen in liquid N_2 immediately. Before analysis, frozen medium was thawed on ice and three sample volumes of ice-cold methanol were added. This was followed by centrifugation (15 min at 12,000 *g* and 4 °C). The supernatant was dried (Savant™ speedvac concentrator and refrigerated condensation trap, Thermo Scientific, Rockford, USA) and stored at −80 °C before use. Before LC-MS analysis, samples were re-suspended in 18 μl of a 4% acetonitrile (ACN) and 0.1% formic acid (FA) solution. LC-MS was performed on a Q Exactive orbitrap mass spectrometer (Thermo Scientific, San Jose, USA), coupled to an Ultimate 3000 ultra-performance liquid chromatography (UPLC) instrument (Thermo Scientific). The UPLC system was equipped with an Easy Spray Pepmap C18 column (75 μm × 25 cm, 3 μm particles, 100 Å pore size; Thermo Scientific, San Jose, CA) and an Acclaim Pepmap C18 pre-column (75 μm × 2 cm, 3 μm particles, 100 Å pore size; Thermo Scientific). Mobile phase A consisted of 99.9% H_2O, 0.1% FA and mobile phase B of 19.9% H_2O, 80% ACN, 0.1% FA. 5 μl of sample was injected at a flow rate of 5 μl/min and 4% of mobile phase B. Metabolite separation was performed using a 22 min gradient at 300 nl/min, where the percentage of mobile phase B increased from 4% to 70% in 20 min and from 70% to 100% in 2 min. Every metabolite separation was followed by a

Please cite this article in press as: Kim, J.-Y., et al., 3D spherical microtissues and microfluidic technology for multi-tissue experiments and analysis. J. Biotechnol. (2015), http://dx.doi.org/10.1016/j.jbiotec.2015.01.003

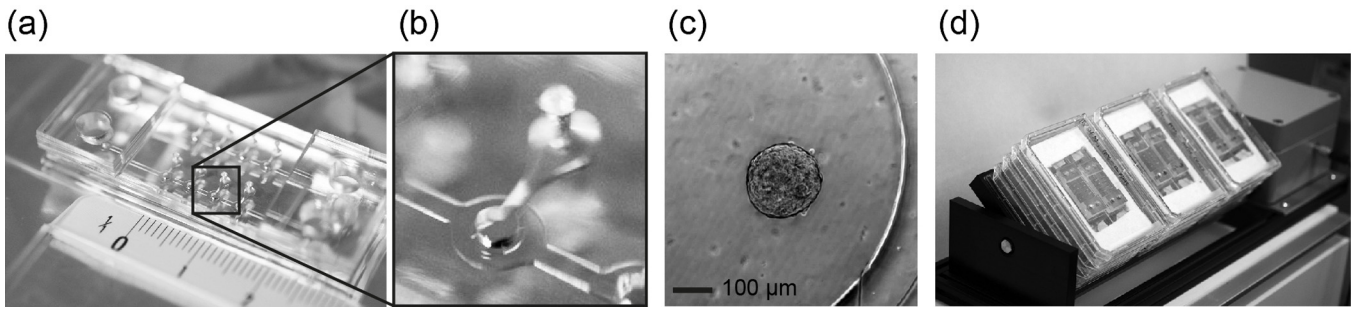

Fig. 2. (a) Photograph of the fabricated chip with (b) enlarged MT compartment, and loading and perfusion channel. (c) HCT116 MT loaded into the compartment. (d) Multiple devices are stacked on a custom-made, automated tilting platform for parallel experiments in a standard CO_2-incubator.

rinse step (5 min gradient, from 4% to 100% of mobile phase B). The Q Exactive mass spectrometer was operated in positive ionization mode. Gas-phase fragmentation was used to increase sensitivity and consisted of 4 consecutive windows of 135–205, 200–255, 250–305 and 300–470 Th. The MS spectra were recorded with a resolving power of 35000 full width at half maximum (FWHM), and the automatic gain control target and maximum injection time were set to 5×10^5 and 100 ms, respectively. Data analysis was performed with MZmine (Pluskal et al., 2010).

3. Results

3.1. Microfluidic device and setup

Fig. 2a illustrates a fabricated device before microtissue loading. It consists of the PDMS structure containing 2 independent channels, which is bonded onto a standard glass slide. An enlarged view of the microtissue compartment is shown in Fig. 2b. It has a height of 550 µm. Clearly visible are the 550-µm-high loading channel with the loading port and the perpendicular medium perfusion channel with a height of 100 µm. We were able to load MTs into the device without any apparent damage, and MTs remained in their compartments during the course of the experiments (Fig. 2c). The initial introduction of medium into the microchannel was facilitated by the Biolipdure coating that renders the PDMS surface hydrophilic. Applied medium is dragged automatically in to the channels due to capillary forces, which is not the case for native PDMS channels. The entrapment of air bubbles in native PDMS channels is common and the bubbles then are difficult to remove. Here the coating helps to prevent the occurrence of bubbles. Two of the described devices were accommodated in a rectangular cell culture plate and placed on the automated tilting platform. Up to 12 plates can be stacked onto the same platform and operated in parallel (Fig. 2d). Therefore, a total number of 48 independent experimental conditions can be executed in parallel in a standard CO_2-incubator. The gravity-driven flow approach does neither require tubing nor pumps, which renders the operation of the overall system simple and robust.

3.2. MT chamber optimization

We experimentally tested different compartment layouts and characterized those by using computational fluid dynamic (CFD) simulations (Fig. 3). For layout No. 1, our experiments evidenced good loading, but the MTs were dragged and squeezed into the perfusion channel despite its height being significantly lower than the diameter of the MTs. In layout No. 2, proper loading was often impossible due to bubbles entrapped in the side pocket. Also, cells frequently adhered to the surface, mainly as a result of inefficient Biolipidure coating. Further, it was unclear, whether medium exchange was efficient on the rear side of the MTs with respect to the perfusion channel. Layout No. 3 showed very reproducible MT loading and stable culturing over the duration of the experiments. Loading the MT directly into the perfusion channel (layout No. 4) in front of a trapping structure led to destruction of the MT in less than a day even at low flow rates due to the large shear forces.

A 3D CFD simulation of layout No. 3 in Fig. 3 shows that the streamlines nicely envelop the complete MT so that an efficient medium turnover in the whole compartment can be anticipated.

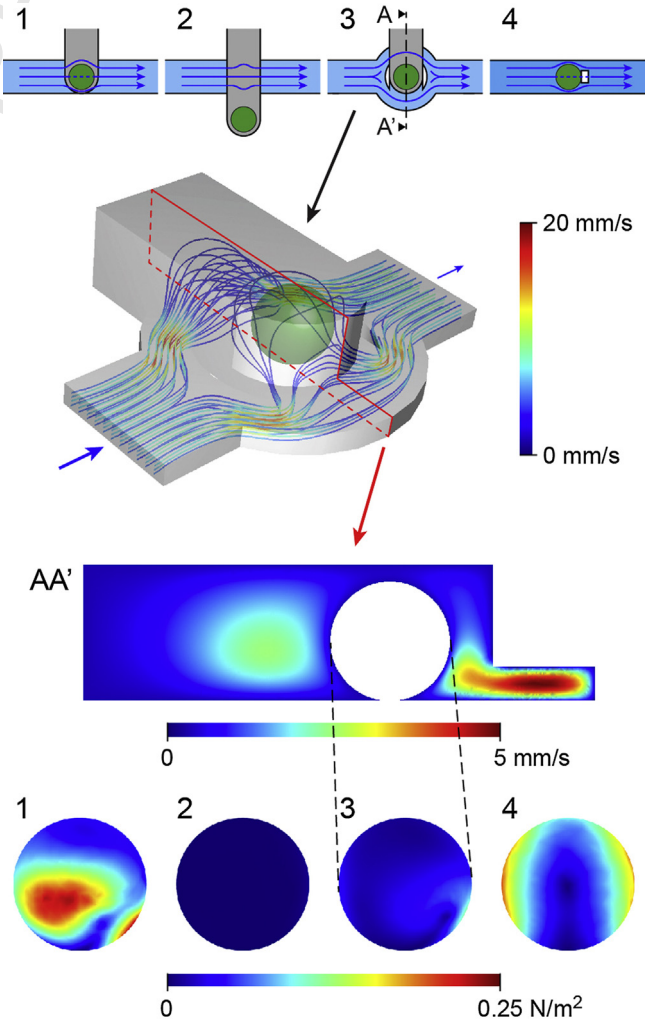

Fig. 3. Four different layouts of the MT compartments were assessed by using CFD simulation. Layout No. 3 combines homogeneous flow around the microtissue with low shear-stress and was, therefore, preferred over the other three microtissue compartment layouts (see Supplementary Fig. S1 for flow speed and shear stress of all layouts).

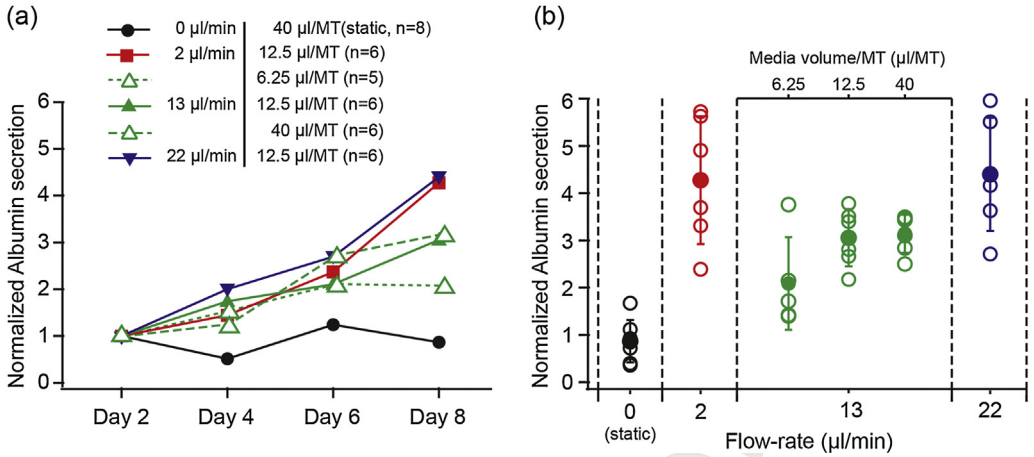

Fig. 4. Functionality of rLiMTs in the microdevice. (a) Albumin secretion of rLiMTs cultured under different perfusion conditions over 8 days in the microchip was measured to be larger than that of rLiMTs cultured under static conditions in a well. (b) Albumin concentrations in the collected supernatants at day 8 (all values plus mean ± s.d.).

Table 1
Mean flow rates as a function of the perfusion channel dimension.

Perfusion channel dimension		Mean flow rates (µl/min)	
Height (µm)	Width (µm)	Model	Experiment
100	80	2.2	1.38
	600	16	13.23
	800	22	23.01

The cross-section AA' depicts the flow-speeds in mm/s. The induced shear stress (N/m^2) on the surface of the spheroid is represented through circular color maps; a frontal view on the spheroids located in the different compartment designs 1–4 is shown. Shear stresses for layout No. 3 are low in comparison to those occurring in design No. 1 & 4, where microtissues are directly exposed to the flow and related shear forces. The simulation results support our choice of layout No. 3 for the MT culturing compartment for the microfluidic chips.

3.3. Control of the perfusion rate

Flow rates were measured for three different widths of the perfusion channel, 80, 600 and 800 µm, which alter the flow resistance of the perfusion channel and, therefore, produce different flow rates for a given inclination angle. Table 1 shows mean flow rates for the first 2 min. It is evident that higher flow rates were obtained for lager channels. The results correspond to calculated flow rates, so that predictions of flow rates can be made for other inclination angles. Gravity-driven perfusion offers great flexibility for controlling the flow in a simple setup. Even though only one inclination angle can be applied for all experimental conditions on the same tilting platform, different flow rates can be achieved by changing perfusion channel widths. Titling the platform back and forth generates bidirectional closed-loop circulation with defined flow reversion. For this paper, 600-µm-wide channels and 25 µl of medium volume were selected as standard perfusion conditions, along with a 2-min tilting interval at 30° inclination. These settings generate a flow rate of approximately 13 µl/min.

3.4. Microfluidic culturing of primary rLiMTs

We cultured rLiMTs under static conditions in wells (GravityTRAP plate) and under perfusion conditions (microfluidic chip) with various flow rates and medium volumes per microtissue over 8 days. MTs preserved their compact morphology over the whole duration of the experiment. No cell adhesion on the PDMS surface was observed. Albumin, a liver-specific marker, secreted by hepatocytes, was measured in the collected supernatants every 2 days. For all perfusion conditions, albumin concentrations increased over time, whereas the albumin secretion rate remained constant over time for MTs cultured in wells (Fig. 4a). Even for the lowest medium volumes in the experiments, 6.25 µl/MT, MTs under perfusion showed higher albumin secretion than MTs cultured in wells, which contained larger medium volumes (40 µl/MT). Different flow rates and medium volumes per MT under perfusion conditions did not cause any decrease in metabolic activity (Fig. 4b). The effect of the flow rate, however, did not show a consistent trend. Importantly, metabolic activity showed only little variation with respect to the medium volumes available to the microtissues, which entails flexibility in the number of MTs that can be loaded into the device.

3.5. Microfluidic bio-activation and effect of cyclophosphamide

Our device allows for loading of different tissue types and enables continuous liquid transfer between the tissue compartments in a closed-loop configuration. Therefore, fluidic networks that connect multiple organotypic 3D microtissue structures can be realized. These networks feature the additional advantage that direct and continuous metabolic transfer between the microtissues can be realized. Continuous liquid-phase interchange can be critical for short-lived metabolites. As a proof of concept experiment, we have chosen a configuration of liver and tumor microtissues. We tested our approach by assessing the bio-activation process of an anticancer pro-drug, cyclophosphamide (CP), under perfusion conditions and under conventional static conditions. Primary rat liver microtissues (rLiMTs) were used as a liver model with the ability to metabolically activate CP by hydroxylation to 4-hydroxy-CP (4OH-CP) through the cytochrome P-450 enzyme (CYP2B enzyme, particularly CYCB1 and CYP2B6). MTs derived from the colon colorectal carcinoma cell line HCT116 were used as tumor model, the effect of the activated drug on which was characterized. 4OH-CP exists with aldophosphamide in equilibrium. Aldophosphamide is easily dissociated to acrolein and phosphoramide mustard (PM), which is a DNA-alkylating agent and kills cancer cells.

3.5.1. Effect of cyclophosphamide on rLiMTs

In a first step, we cultured rLiMTs without tumor tissues under different CP concentrations (0, 0.1 and 1 mM) over 8 days to investigate the direct toxicity of CP on rLiMTs under perfusion and static conditions. Approximately 8.33 µl/MT (3 rLiMTs in 25 µl medium) of medium was perfused at a flow rate of 13 µl/min. Fig. 5a shows

Please cite this article in press as: Kim, J.-Y., et al., 3D spherical microtissues and microfluidic technology for multi-tissue experiments and analysis. J. Biotechnol. (2015), http://dx.doi.org/10.1016/j.jbiotec.2015.01.003

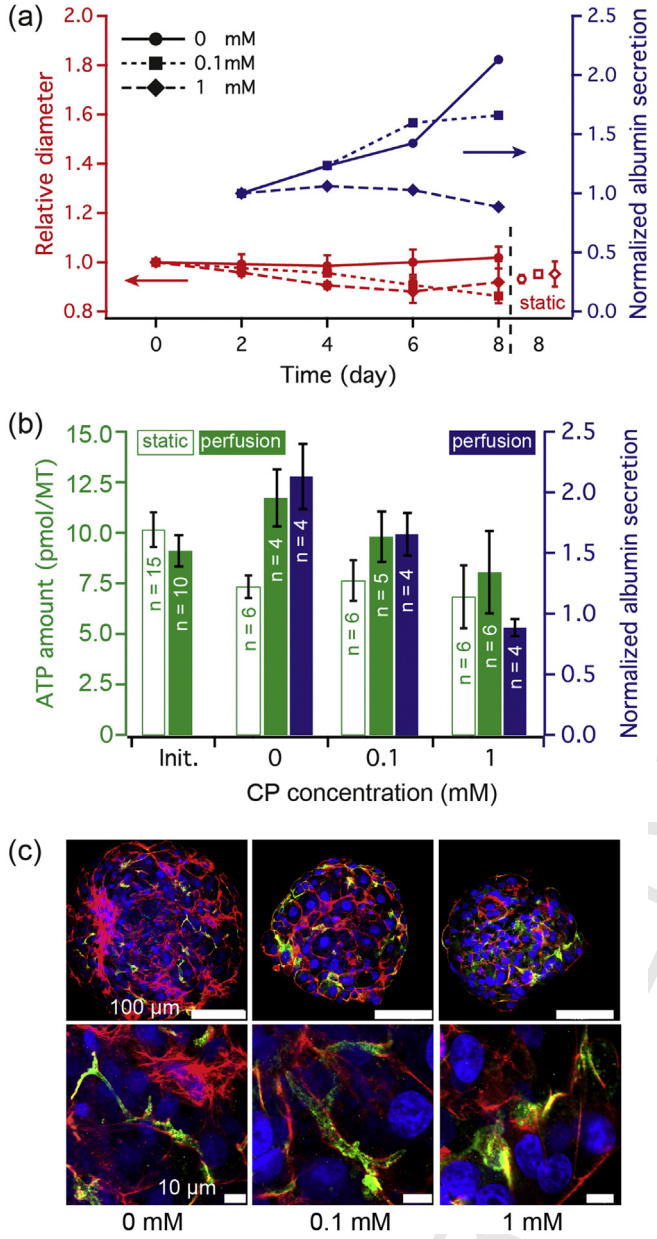

Fig. 5. Primary rLiMTs cultured in different CP concentrations (0, 0.1, 1.0 mM). (a) Only a slight decrease in diameter over 8 days was observed in continuous-perfusion and static cultures (relative to day 0, means ± s.d., $n = 12$, 1 Exp.). Whereas an expected increase of the albumin secretion was measured for low CP concentrations, albumin secretion remained relatively constant for 1.0 mM CP over 8 days (means, normalized to day 2, $n = 4$). (b) ATP content and albumin secretion on day 8 for perfused and static cultures (mean ± s.d., n-values as indicated). (c) rLiMTs were fixed and incubated with an antibody against DPP IV to mark the bile canaliculi (green), phalloidin-rhodamine (red) to visualize the actin cytoskeleton, and DAPI (blue) to counterstain the nucleus. Images were captured using a confocal laser scanning microscope (Olympus) using a 40× objective (upper panel), which were zoomed in to obtain a more detailed view of the canalicular structures (bottom panel).

relative diameters of rLiMTs (red curves, left y-axis) and albumin secretion values (blue curves, right y-axis) over the 8 days. We observed only a minor decrease in size and small differences in the morphology of rLiMTs cultured in CP containing medium in comparison to medium without CP. Static cultures featured a small reduction in MT diameter under all conditions. The increasing secretion of albumin previously observed in perfused culturing was reduced at higher CP concentrations. With a concentration of 1 mM CP present in the medium, the secretion was relatively constant over 8 days, and was slightly lower on day 8 (Fig. 5b). The same outcome was obtained when comparing the ATP contents of rLiMTs after they had been removed from the microfluidic devices at day 8 (Fig. 5b, filled green bars, left y-axis). Static cultures featured a slightly lower MT viability under all conditions (Fig. 5b, empty green bars, left y-axis). Perfused rLiMTs were further analyzed by immunostaining by using antibodies directed against DPPIV to visualize bile canaliculi and phalloidin to stain the actin cytoskeleton (Fig. 5c). The control rLiMT (0 mM CP) formed bile canaliculi (green). Phalloidin (red) stained the cell boundary, which is characteristic of differentiated hepatocytes (Godoy et al., 2013). CP exposure resulted in a small decrease in microtissue size, supporting the diameter measurements in Fig. 5a (upper panel). In addition, there is evidence of altered morphology of the bile canaliculi that appeared to be enlarged (lower panel).

In conclusion, the presence of CP in the culturing medium generally affects rLiMTs, specifically size, viability and metabolic activity. For concentrations of 1 mM CP and lower, however, rLiMTs still show cell-specific functionality, which is comparable to that of rLiMTs in conventional well-cultures without CP. This holds for a period of at least 8 days.

3.5.2. Effect of cyclophosphamide on HCT116 MTs

In a second step, we cultured our target tumor model, HCT116 MTs, without rLiMTs over 8 days under static and perfusion conditions to investigate the impact of non-metabolized CP on the tumor. For the static culturing conditions, HCT116 MTs were cultured at 0 and 1 mM CP in 96-well plates (50 µl/min). For perfusion conditions, one HCT116 MT per channel was loaded into the chip and cultured in 25 µl medium containing 0, 0.1 and 1 mM CP. Growth rates of the MTs were slightly lower (approximately 10%) for both culturing methods in medium containing 1 mM CP as compared to medium without any CP (Fig. 6a). Bright-field microscopy images at day 8 (Fig. 6b) revealed no significant differences. MTs cultured in perfused medium containing 0 mM, 0.1 mM as well as 1 mM CP showed similar sizes and morphologies. The viability of the HCT116 MTs slightly decreased with increasing CP concentrations in the medium (Fig. 6c). Again, no significant differences were observed between static and perfusion conditions. Similarly, the ATP content of HCT116 MTs was approximately 20% lower when MTs were cultured in the presence on 1 mM CP in the medium as compared to culturing without CP in the medium. The MTs were further analyzed by confocal microscopy using phalloidin to stain the actin cytoskeleton. In agreement with the measured diameter and bright-field images (Fig. 6a and b), no change in MT size was observed, even with 1 mM CP (Fig. 6d). In addition, there appears not to be any major difference in cytoskeletal structure as evidenced by phalloidin staining. This is even more obvious in the single-color images with phalloidin, where the architecture appears unchanged as compared to the control (Fig. S2 in the Supplementary data).

3.5.3. Effect of cyclophosphamide on HCT116 MTs co-cultured with rLiMTs

Liver and tumor MTs were cultured in the presence of different CP concentrations in wells and under microfluidic perfusion conditions. These experiments were intended to characterize the importance of fluidic communication between the two different MT types and the potential effects of bio-activated CP on the tumor MTs. For static condition, 6 rLiMTs were pooled in 96-well plates and exposed to medium containing CP. After 2 days, medium from these wells was manually transferred into wells each containing one HCT116 MT. The liver MT pooling procedure had to be repeated every 2 days, since rLiMTs close to each other merged within less than 2 days, which may cause metabolic activities that are difficult

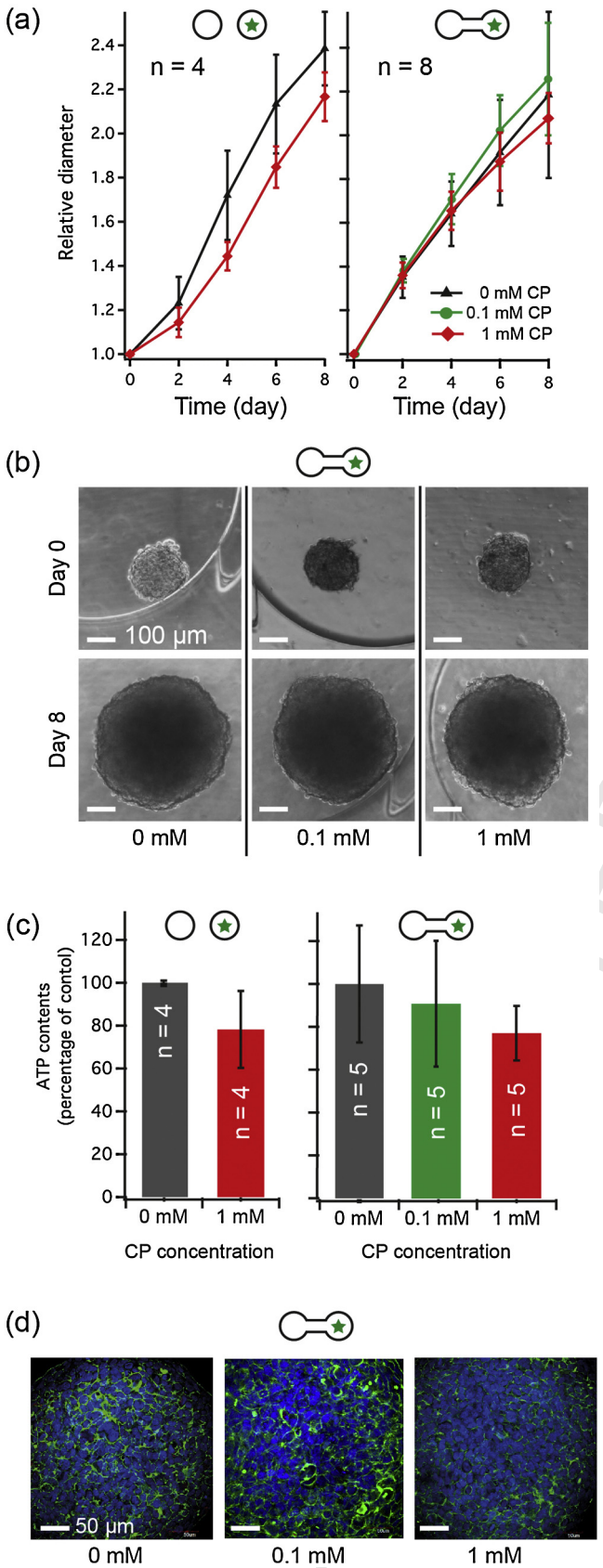

Fig. 6. Effect of CP on HCT116 MTs alone (no liver). (a) Relative diameter (normalized with respect to day 0) of HCT116 MTs cultured over 8 days under static (1 Exp.) and microfluidic (2 Exps.) conditions with and without 1 mM CP. Slightly lower growth was observed for 1 mM CP (means ± s.d.). (b) Bright-field images of HCT116 MT at day 0 and day 8 in the microfluidic chip showed comparable MT morphologies for all three CP concentrations. (c) A lower ATP content (–20%) was measured in HCT116 MTs at day 8 (mean ± s.d.) upon culturing in medium with 1 mM CP for both methods. (d) After 8 days on the chip, MTs were fixed and incubated with Alexa Fluor® 488 Phalloidin (green) to visualize the actin cytoskeleton and DAPI (blue) to counterstain the nucleus. Images were captured using a confocal laser scanning microscope (Olympus) using a 40× (see also Fig. S2).

to predict, as the structure of the microtissues drastically changes. The medium was exchanged every 2 days. The medium volume per MT amounted in all cases to 8.33 µl/rLiMT, for further details, see materials and methods section.

While no significant effect on HCT116 MTs was observed under static conditions, clear consequences of CP exposure were recognized under perfusion conditions. The diameter of HCT116 MTs in wells with medium transfer by pipetting was not decreased for any of the CP concentrations (Fig. 7a and b). However, stagnation and even reduction of the MT diameter was observed for HCT116 MTs cultured together with rLiMTs under perfusion conditions in the microchip in medium containing 1 mM of CP. MTs cultured in the microfluidic chip in medium containing 0 and 0.1 mM CP showed unchanged diameters. This finding was supported by the ATP contents of the HCT116 MTs at the end of the experiment on day 8 (Fig. 7c). Under static conditions, the viability of HCT116 MTs decreased to about 80% with respect to control in the presence of media collected from rLiMTs incubated with 1 mM CP. This value corresponds to the direct toxicity of CP on HCT116 MT that was measured before (Fig. 6b). The preconditioning of the medium with rLiMTs, therefore, has no additional effect on the diameter of HCT116 MTs. The effect of bioactivation in wells can only be minor. In contrast, the viability decreased to about 50% over the period of 8 days, when HCT116 were co-cultured with rLiMTs in the same microfluidic environment under perfusion conditions in the presence of 1 mM CP. Again, no viability decrease was measured in controls and with 0.1 mM of CP in the medium. To characterize the morphology of the HCT116 MTs, phalloidin staining was performed. As shown in Fig. 7d, even after incubation with 1 mM CP, phalloidin localized to the tumor cell periphery with no major change in tumor cell morphology (see also Fig. S3 in the Supplementary data). This finding indicates that CP most probably did not cause any cytotoxic effects but just slowed down tumor cell proliferation.

Medium samples collected at day 8 of the experiment were analyzed by using mass spectrometry. The mass range between 135–470 m/z (mass to charge ratio) was screened for metabolites of CP (see Fig. 8). Metabolites (MH^+) were identified by accurate mass matching (<3 ppm), and the ion count was based on the extracted ion chromatogram of each metabolite. CP was measured in samples of HCT116 only and HCT116 + rLiMT configurations treated with 0.1 and 1 mM CP in a concentration-dependent manner. 4OH-CP and aldophosphamide are isomers and have exactly the same mass and could not be differentiated in this study. A mass corresponding to 4OH-CP/aldophosphamide was detected in the 1 mM CP treated HCT116 + rLiMT samples. Further, several metabolites originating from 4OH-CP were detected, including 4-ketocyclophosphamide and iminocyclophosphamide, again only in 1 mM CP treated HCT116 + rLiMT samples, indirectly indicating the presence of 4OH-CP. The presence of aldophosphamide was confirmed by carboxyphosphamide and alcophosphamide (see Table S1 in Supplementary data). Importantly, none of the metabolites was detected in the HCT116 only configuration, which confirms liver-specific bio-activation of CP.

4. Discussion

Combining 3D tissue engineering with microfluidic technology poses a multitude of challenges. Many of the methods for the production of 3D tissue structures that are currently developed

Please cite this article in press as: Kim, J.-Y., et al., 3D spherical microtissues and microfluidic technology for multi-tissue experiments and analysis. J. Biotechnol. (2015), http://dx.doi.org/10.1016/j.jbiotec.2015.01.003

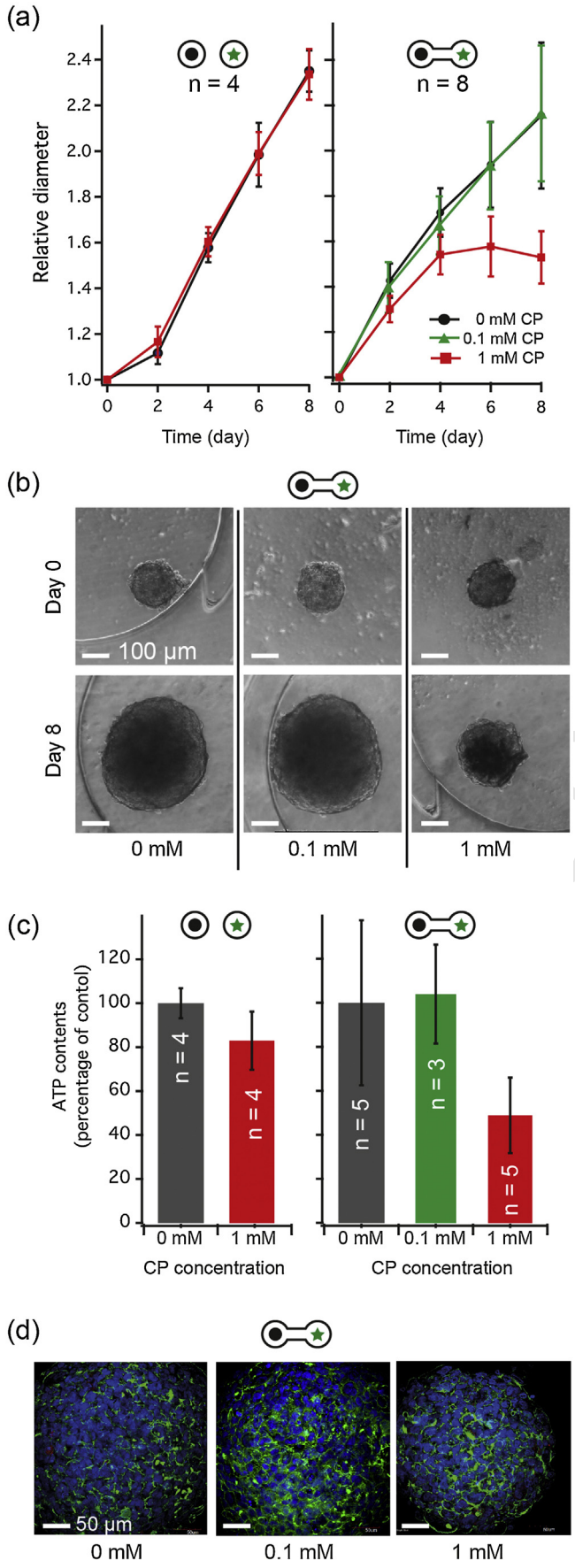

Fig. 7. Bio-activation of CP and effect on tumor MTs. (a) A significant growth reduction of HCT116 MTs was observed over 8 days when cultured in microfluidic conditions (2 Exps.) under the presence of 1 mM CP (relative diameter, normalized to day 0). Lower CP concentrations (<0.1 mM) and cultures in wells (1 Exp.) showed no effect compared to control experiments (means ± s.d.). (b) Significant differences in the diameter of the tumor spheroids cultured for 8 days in different CP concentrations are visible in bright-field micrographs. (c) ATP contents of HCT116 MT at day 8 (mean ± s.d., relative to 0 mM). (d) Immunostaining by Alexa Fluor® 488 Phalloidin (green) of MT cultivated on the chip for 8 days to visualize the actin cytoskeleton. The conditions described in Fig. 6d were applied (see also Fig. S3).

and optimized are not compatible with microfluidic networks. Microtissues can either be produced off-chip and loaded into the microfluidic network or directly formed in a micro-compartment on chip. The 3D tissue formation has to be simple, robust and reproducible and may not restrict the layout of the microfluidic chip for exposure experiments too much. For routine implementation, the microfluidic culturing devices have to be simple to fabricate. They should be easy to use, albeit provide reliable and reproducible culturing conditions and should be amenable to standard read-out methods. Most importantly, the morphology of the microtissues and their organ-specific functionality has to be preserved for extended times in culture, preferably equal to or longer than that of existing microwell methods.

Our approach presented in this article has several advantages: (i) Spheroids as 3D tissue model give access to a multitude of different organ models, which are based on the same fabrication technology and can be handled similarly in microfluidic structures; (ii) Off-chip spheroid fabrication can be completely decoupled from in-chip cultivation, so that tissue fabrication complexity does not impact the layout of the microfluidic chip for experiments. This separation makes the whole platform much more flexible with regard to potential tissue formation methods, tissue loading, analysis and retrieval for further detailed downstream analysis. This holds particularly true in comparison to tissue structures based on scaffolds, such as hydrogels, which have to be adapted to each individual cell type; (iii) Gravity-based loading is simple, does not require external actuation and allows for precise placement of the MTs in the perfusion microchannel network; (iv) The gravity-induced flow concept based on two open reservoirs without any tubing allows for robust closed-loop perfusion, simple medium exchange, and liquid sampling. It also features inherent gas exchange (CO_2, O_2). No air bubbles – a frequent and severe problem in microfluidic setups – perturb the flow and tissue cultures. Evaporation from the reservoirs can be kept at a minimum by placing the microchips in a humidified atmosphere; (v) The automated tilting setup is compatible with sterile culture conditions and allows for robust operation in a conventional incubator over several days; (vi) During experiments, spheroids can be inspected and analyzed optically; they can be accessed after the experiment for further analysis.

The simple microfluidic layout with individual culturing compartments already allows for a very flexible arrangement of different tissue types, without the risk that they merge. Other microfluidic networks for a higher number of tissues and for reproducing physiologically relevant orders in multi-tissue experiments are conceivable. The versatile platform presented here enables reproducible multi-tissue experiments. Its simple fabrication and operation provides a high reproducibility for different conditions and enables parallelization of experiments.

Spheroids derived from freshly isolated rat liver cells were cultured in the microfluidic chip over more than a week without losing their morphology and functionality. Yet, rLiMTs showed higher albumin secretion rates, and, consequently, larger metabolic activity under microfluidic perfusion conditions as compared to MTs cultured in wells, in which more medium volume is available. Potential reasons may include increased medium exchange, nutrient supply, and waste removal in the vicinity of the MTs

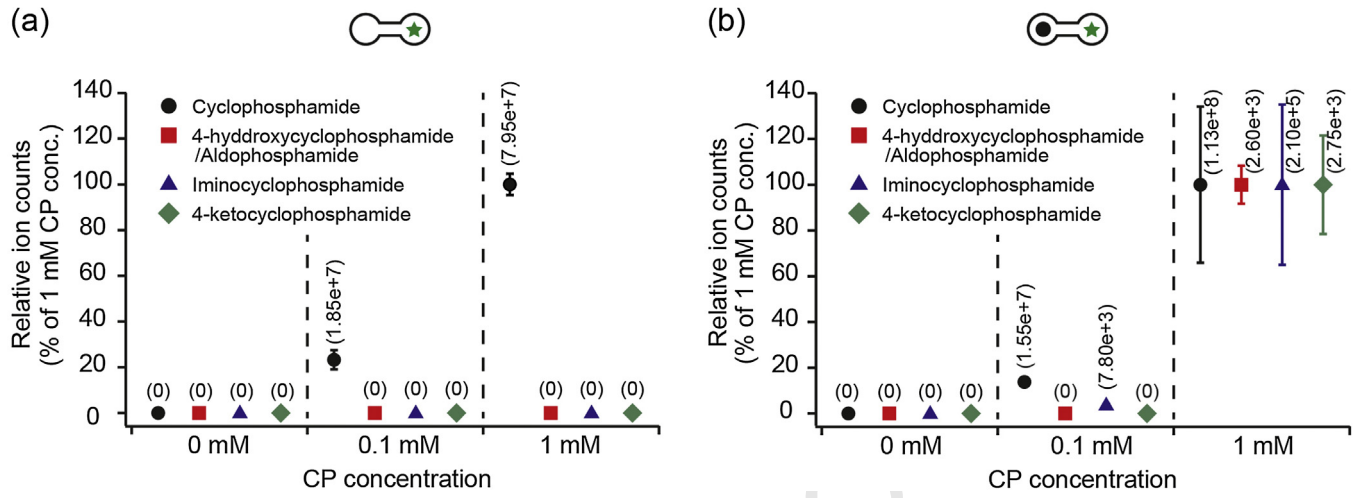

Fig. 8. MS data of the supernatants of HCT116 MTs cultured with and without liver collected at day 8 (a) For the perfused HCT116-only configuration CP was detected in a concentration-dependent manner. None of the metabolites was detected. (b) For perfused HCT116 + rLiMT CP was measured again. For 1 mM CP several metabolites of CP such as 4OH-CP, aldophosphamide, iminocyclophosphamide and 4-ketocyclophosphamide were additionally detected in the supernatants (ion counts plotted relative to 1 mM CP samples; absolute ion counts are in brackets).

through convection under perfusion conditions. Under static conditions, nutrient supply and waste removal are only possible through diffusion-controlled medium exchange. The Biolipidure coating efficiently prevented cell adhesion for more than a week. A common problem in microfluidic cell cultures and toxicity studies is compound adsorption at walls and absorption into the permeable PDMS substrate. For albumin and CP we found that this effect was significantly reduced by the surface coating. CP has been detected in the supernatant at expected concentrations through MS analysis. Albumin concentrations measured in the microchip samples were comparable to those of other studies and those of our well cultures, in which the same coating has been applied. Ad- or absorption of other compounds that are present at low concentrations has to be further investigated.

With our microfluidic setup we were able to conduct a 3D multi-tissue experiment by using microtissues made from two different cell types that were fluidically connected inside the chip for direct metabolite transfer. Only continuous interaction and liquid exchange reproduced the effect of liver-tissue-mediated bioactivation of cyclophosphamide that then affected the growth of the tumor tissue, whereas control experiments as well as discrete medium transfer experiments did not evidence any effect. These results have been confirmed by confocal imaging and MS analysis of collected samples. The concentrations of cyclophosphamide used in this study (0.1–1 mM) include the *in vivo* relevant range. For example, plasma peak concentrations of 0.15 mM cyclophosphamide have been reported for patients after administration of 1000 mg/m^2 body surface (Struck et al., 1987), a dose typically used in clinical routine (Hengstler et al., 1999). Since cyclophosphamide is often used at even higher doses, such as 1800 mg/m^2, it can be expected that the peak blood concentrations in patients usually reach the concentration range of 0.1–1 mM tested here. In previous studies we have used genetically engineered cells expressing cytochrome P4502B1, an enzyme metabolically activating cyclophosphamide for cytostatic drug testing (Hengstler et al., 1997). In this *in vitro* system concentrations higher than 4 mM cyclophosphamide had to be used to induce cytotoxic effects. This example illustrates that the here established body-on-a-chip configuration allows an efficient activation of cyclophosphamide to cytotoxic metabolites and sensitive toxicity testing at *in vivo* relevant concentrations.

5. Conclusions

We presented an automatable microfluidic platform for parallelized and reproducible multi-tissue experiments on the basis of 3D multi-cellular spheroids. The system allowed for reproducing bio-activation effects known from *in vivo* experiments while achieving significant down scaling with respect to medium volume and cell numbers. The bio-activation results prove the feasibility of our approach and pave the way towards more complex experiments in "body-on-a-chip" formats while retaining low complexity in tissue handling and experiments.

Author contributions

J.-Y.K. fabricated the devices, performed microfluidic experiments and analyzed the data, and wrote the manuscript; D.A.F. contributed to the experimental design, performed part of the experiments and provided all primary cell material; R.M. performed MT staining and confocal imaging; K.B. performed mass spectrometry experiments; S.M. and P.S. fabricated the devices and performed initial microfluidic experiments; J.G.H. edited the manuscript and proposed the concept for the bio-activation experiments; J.M.K. edited the manuscript and was involved in experimental design and scientific considerations; A.H. contributed to the overall project concept and writing of the manuscript; O.F. conceived the tilting chip concept, designed, fabricated and optimized the microfluidic devices including CFD simulations, analyzed data and wrote the manuscript; All authors discussed the results and implications and commented on the manuscript at all stages.

Acknowledgements

This work was financially supported by the FP7 of the EU through the project "Body on a chip", ICT-FET-296257, by the FP7 EU project DETECTIVE (SEURAT-1) and an individual Ambizione Grant 142440 of the Swiss National Science Foundation for Olivier Frey. Sirion Biotech is acknowledged for providing the HCT116 eGFP cell line. The authors thank Wolfgang Moritz, InSphero AG, for comments and input throughout the study.

Appendix A. Supplementary data

Supplementary data associated with this article can be found, in the online version, at http://dx.doi.org/10.1016/j.jbiotec.2015.01.003.

References

Abbott, A., 2003. Cell culture: biology's new dimension. Nature 424, 870–872, http://dx.doi.org/10.1038/424870a.

Dittrich, P.S., Manz, A., 2006. Lab-on-a-chip: microfluidics in drug discovery. Nat. Rev. Drug Discov. 5, 210–218, http://dx.doi.org/10.1038/nrd1985.

Drewitz, M., Helbling, M., Fried, N., Bieri, M., Moritz, W., Lichtenberg, J., Kelm, J.M., 2011. Towards automated production and drug sensitivity testing using scaffold-free spherical tumor microtissues. Biotechnol. J. 6, 1488–1496, http://dx.doi.org/10.1002/biot.201100290.

El-Ali, J., Sorger, P.K., Jensen, K.F., 2006. Cells on chips. Nature 442, 403–411, http://dx.doi.org/10.1038/nature05063.

Esch, M.B., King, T.L., Shuler, M.L., 2011. The role of body-on-a-chip devices in drug and toxicity studies. Annu. Rev. Biomed. Eng. 13, 55–72, http://dx.doi.org/10.1146/annurev-bioeng-071910-124629.

Esch, M.B., Smith, A.S.T., Prot, J.-M., Oleaga, C., Hickman, J.J., Shuler, M.L., 2014. How multi-organ microdevices can help foster drug development. Adv. Drug Deliv. Rev. 69–70, 158–169, http://dx.doi.org/10.1016/j.addr.2013.12.003.

Friedrich, J., Ebner, R., Kunz-Schughart, L.a., 2007. Experimental anti-tumor therapy in 3-D: spheroids–old hat or new challenge? Int. J. Radiat. Biol. 83, 849–871, http://dx.doi.org/10.1080/09553000701727531.

Frimat, J.-P., Becker, M., Chiang, Y.-Y., Marggraf, U., Janasek, D., Hengstler, J.G., Franzke, J., West, J., 2011. A microfluidic array with cellular valving for single cell co-culture. Lab Chip 11, 231–237, http://dx.doi.org/10.1039/c0lc00172d.

Frimat, J.-P., Sisnaiske, J., Subbiah, S., Menne, H., Godoy, P., Lampen, P., Leist, M., Franzke, J., Hengstler, J.G., van Thriel, C., West, J., 2010. The network formation assay: a spatially standardized neurite outgrowth analytical display for neurotoxicity screening. Lab Chip 10, 701–709, http://dx.doi.org/10.1039/b922193j.

Frisk, T., Rydholm, S., Andersson, H., Stemme, G., Brismar, H., 2005. A concept for miniaturized 3-D cell culture using an extracellular matrix gel. Electrophoresis 26, 4751–4758, http://dx.doi.org/10.1002/elps.200500478.

Ghafar-Zadeh, E., Waldeisen, J.R., Lee, L.P., 2011. Engineered approaches to the stem cell microenvironment for cardiac tissue regeneration. Lab Chip 11, 3031–3048, http://dx.doi.org/10.1039/c1lc20284g.

Ghallab, A., 2013. In vitro test systems and their limitations. EXCLI J. 12, 1024–1026.

Godoy, P., Hewitt, N.J., Albrecht, U., Andersen, M.E., Ansari, N., Bhattacharya, S., Bode, J.G., Bolleyn, J., Borner, C., Böttger, J., Braeuning, A., Budinsky, R.A., Burkhardt, B., Cameron, N.R., Camussi, G., Cho, C.-S., Choi, Y.-J., Craig Rowlands, J., Dahmen, U., Damm, G., Dirsch, O., Donato, M.T., Dong, J., Dooley, S., Drasdo, D., Eakins, R., Ferreira, K.S., Fonsato, V., Fraczek, J., Gebhardt, R., Gibson, A., Glanemann, M., Goldring, C.E.P., Gómez-Lechón, M.J., Groothuis, G.M.M., Gustavsson, L., Guyot, C., Hallifax, D., Hammad, S., Hayward, A., Häussinger, D., Hellerbrand, C., Hewitt, P., Hoehme, S., Holzhütter, H.-G., Houston, J.B., Hrach, J., Ito, K., Jaeschke, H., Keitel, V., Kelm, J.M., Kevin Park, B., Kordes, C., Kullak-Ublick, G.A., LeCluyse, E.L., Lu, P., Luebke-Wheeler, J., Lutz, A., Maltman, D.J., Matz-Soja, M., McMullen, P., Merfort, I., Messner, S., Meyer, C., Mwinyi, J., Naisbitt, D.J., Nussler, A.K., Olinga, P., Pampaloni, F., Pi, J., Pluta, L., Przyborski, S.A., Ramachandran, A., Rogiers, V., Rowe, C., Schelcher, C., Schmich, K., Schwarz, M., Singh, B., Stelzer, E.H.K., Stieger, B., Stöber, R., Sugiyama, Y., Tetta, C., Thasler, W.E., Vanhaecke, T., Vinken, M., Weiss, T.S., Widera, A., Woods, C.G., Xu, J.J., Yarborough, K.M., Hengstler, J.G., 2013. Recent advances in 2D and 3D in vitro systems using primary hepatocytes, alternative hepatocyte sources and non-parenchymal liver cells and their use in investigating mechanisms of hepatotoxicity, cell signaling and ADME. Arch. Toxicol. 87, 1315–1530, http://dx.doi.org/10.1007/s00204-013-1078-5.

Griffith, L.G., Swartz, M.a., 2006. Capturing complex 3D tissue physiology in vitro. Nat. Rev. Mol. Cell Biol. 7, 211–224, http://dx.doi.org/10.1038/nrm1858.

Hammad, S., 2013. Advances in 2D and 3D in vitro systems for hepatotoxicity testing. EXCLI J. 12, 993–996.

Hammad, S., Hoehme, S., Friebel, A., von Recklinghausen, I., Othman, A., Begher-Tibbe, B., Reif, R., Godoy, P., Johann, T., Vartak, A., Golka, K., Bucur, P.O., Vibert, E., Marchan, R., Christ, B., Dooley, S., Meyer, C., Ilkavets, I., Dahmen, U., Dirsch, O., Böttger, J., Gebhardt, R., Drasdo, D., Hengstler, J.G., 2014. Protocols for staining of bile canalicular and sinusoidal networks of human, mouse and pig livers, three-dimensional reconstruction and quantification of tissue microarchitecture by image processing and analysis. Arch. Toxicol. 88, 1161–1183, http://dx.doi.org/10.1007/s00204-014-1243-5.

Hengstler, J.G., Hengst, A., Fuchs, J., Tanner, B., Pohl, J., Oesch, F., 1997. Induction of DNA crosslinks and DNA strand lesions by cyclophosphamide after activation by cytochrome P450 2B1. Mutat. Res. 373, 215–223.

Hengstler, J.G., Lange, J., Kett, A., Dornhöfer, N., Meinert, R., Arand, M., Knapstein, P.G., Becker, R., Oesch, F., Tanner, B., 1999. Contribution of c-erbB-2 and topoisomerase IIalpha to chemoresistance in ovarian cancer. Cancer Res. 59, 3206–3214.

Hirschhaeuser, F., Menne, H., Dittfeld, C., West, J., Mueller-Klieser, W., Kunz-Schughart, L.a., 2010. Multicellular tumor spheroids: an underestimated tool is catching up again. J. Biotechnol. 148, 3–15, http://dx.doi.org/10.1016/j.jbiotec.2010.01.012.

Hsiao, A.Y., Torisawa, Y., Tung, Y.-C., Sud, S., Taichman, R.S., Pienta, K.J., Takayama, S., 2009. Microfluidic system for formation of PC-3 prostate cancer co-culture spheroids. Biomaterials 30, 3020–3027, http://dx.doi.org/10.1016/j.biomaterials.2009.02.047.

Hsiao, A.Y., Tung, Y.-C., Qu, X., Patel, L.R., Pienta, K.J., Takayama, S., 2012. 384 hanging drop arrays give excellent Z-factors and allow versatile formation of co-culture spheroids. Biotechnol. Bioeng. 109, 1293–1304.

Huang, S.-B., Wu, M.-H., Wang, S.-S., Lee, G.-B., 2011. Microfluidic cell culture chip with multiplexed medium delivery and efficient cell/scaffold loading mechanisms for high-throughput perfusion 3-dimensional cell culture-based assays. Biomed. Microdevices 13, 415–430, http://dx.doi.org/10.1007/s10544-011-9510-1.

Huh, D., Hamilton, G.a., Ingber, D.E., 2011. From 3D cell culture to organs-on-chips. Trends Cell Biol. 21, 745–754, http://dx.doi.org/10.1016/j.tcb.2011.09.005.

Imura, Y., Sato, K., Yoshimura, E., 2010. Micro total bioassay system for ingested substances: assessment of intestinal absorption, hepatic metabolism, and bioactivity. Anal. Chem. 82, 9983–9988, http://dx.doi.org/10.1021/ac100806x.

Ishihara, K., Ziats, N.P., Tierney, B.P., Nakabayashi, N., Anderson, J.M., 1991. Protein adsorption from human plasma is reduced on phospholipid polymers. J. Biomed. Mater. Res. 25, 1397–1407, http://dx.doi.org/10.1002/jbm.820251107.

Jin, H.-J., Cho, Y.-H., Gu, J.-M., Kim, J., Oh, Y.-S., 2011. A multicellular spheroid formation and extraction chip using removable cell trapping barriers. Lab Chip 11, 115–119, http://dx.doi.org/10.1039/c0lc00134a.

Kachouie, N.N., Du, Y., Bae, H., Khabiry, M., Ahari, A.F., Zamanian, B., Fukuda, J., Khademhosseini, A., 2010. Directed assembly of cell-laden hydrogels for engineering functional tissues. Organogenesis 6, 234–244, http://dx.doi.org/10.4161/org.6.4.12650.

Kampe, T., König, A., Schroeder, H., Hengstler, J.G., Niemeyer, C.M., 2014. Modular microfluidic system for emulation of human phase I/phase II metabolism. Anal. Chem. 86, 3068–3074, http://dx.doi.org/10.1021/ac404128k.

Kelm, J.M., Fussenegger, M., 2004. Microscale tissue engineering using gravity-enforced cell assembly. Trends Biotechnol. 22, 195–202, http://dx.doi.org/10.1016/j.tibtech.2004.02.002.

Kelm, J.M., Timmins, N.E., Brown, C.J., Fussenegger, M., Nielsen, L.K., 2003. Method for generation of homogeneous multicellular tumor spheroids applicable to a wide variety of cell types. Biotechnol. Bioeng. 83, 173–180, http://dx.doi.org/10.1002/bit.10655.

Khademhosseini, A., Langer, R., Borenstein, J., Vacanti, J.P., 2006. Microscale technologies for tissue engineering and biology. Proc. Natl. Acad. Sci. USA 103, 2480–2487, http://dx.doi.org/10.1073/pnas.0507681102.

Kim, M.S., Yeon, J.H., Park, J.-K., 2007. A microfluidic platform for 3-dimensional cell culture and cell-based assays. Biomed. Microdevices 9, 25–34, http://dx.doi.org/10.1007/s10544-006-9016-4.

Kim, T., Doh, I., Cho, Y.-H., 2012. On-chip three-dimensional tumor spheroid formation and pump-less perfusion culture using gravity-driven cell aggregation and balanced droplet dispensing. Biomicrofluidics 6, 034107, http://dx.doi.org/10.1063/1.4739460.

Kovarik, M.L., Gach, P.C., Ornoff, D.M., Wang, Y., Balowski, J., Farrag, L., Allbritton, N.L., 2012. Micro total analysis systems for cell biology and biochemical assays. Anal. Chem. 84, 516–540, http://dx.doi.org/10.1021/ac202611x.

Leclerc, E., Sakai, Y., Fujii, T., 2003. Cell culture in 3-dimensional microfluidic structure of PDMS. Biomed. Microdevices 5, 109–114, http://dx.doi.org/10.1023/A:1024583026925.

Lee, J., Cuddihy, M.J., Kotov, N.a., 2008. Three-dimensional cell culture matrices: state of the art. Tissue Eng. Part B. Rev. 14, 61–86, http://dx.doi.org/10.1089/teb.2007.0150.

Lee, P.J., Hung, P.J., Lee, L.P., 2007. An artificial liver sinusoid with a microfluidic endothelial-like barrier for primary hepatocyte culture. Biotechnol. Bioeng. 97, 1340–1346, http://dx.doi.org/10.1002/bit.21360.

Mazzoleni, G., Di Lorenzo, D., Steimberg, N., 2009. Modelling tissues in 3D: the next future of pharmaco-toxicology and food research? Genes Nutr. 4, 13–22, http://dx.doi.org/10.1007/s12263-008-0107-0.

Messner, S., Agarkova, I., Moritz, W., Kelm, J.M., 2013. Multi-cell type human liver microtissues for hepatotoxicity testing. Arch. Toxicol. 87, 209–213, http://dx.doi.org/10.1007/s00204-012-0968-2.

Pampaloni, F., Reynaud, E.G., Stelzer, E.H.K., 2007. The third dimension bridges the gap between cell culture and live tissue. Nat. Rev. Mol. Cell Biol. 8, 839–845, http://dx.doi.org/10.1038/nrm2236.

Pampaloni, F., Stelzer, E., 2010. Three-dimensional cell cultures in toxicology. Biotechnol. Genet. Eng. Rev. 26, 117–138.

Pluskal, T., Castillo, S., Villar-Briones, A., Oresic, M., 2010. MZmine 2: modular framework for processing, visualizing, and analyzing mass spectrometry-based molecular profile data. BMC Bioinformatics 11, 395, http://dx.doi.org/10.1186/1471-2105-11-395.

Powers, M.J., Janigian, D.M., Wack, K.E., Baker, C.S., Beer Stolz, D., Griffith, L.G., 2002. Functional behavior of primary rat liver cells in a three-dimensional perfused microarray bioreactor. Tissue Eng. 8, 499–513, http://dx.doi.org/10.1089/107632702760184745.

Rimann, M., Graf-Hausner, U., 2012. Synthetic 3D multicellular systems for drug development. Curr. Opin. Biotechnol. 23, 803–809, http://dx.doi.org/10.1016/j.copbio.2012.01.011.

Ringel, M., von Mach, M.A., Santos, R., Feilen, P.J., Brulport, M., Hermes, M., Bauer, A.W., Schormann, W., Tanner, B., Schön, M.R., Oesch, F., Hengstler, J.G., 2005. Hepatocytes cultured in alginate microspheres: an optimized technique to study enzyme induction. Toxicology 206, 153–167, http://dx.doi.org/10.1016/j.tox.2004.07.017.

Ruppen, J., Cortes-Dericks, L., Marconi, E., Karoubi, G., Schmid, R.A., Peng, R., Marti, T.M., Guenat, O.T., 2014. A microfluidic platform for chemoresistive

testing of multicellular pleural cancer spheroids. Lab Chip 14, 1198–1205, http://dx.doi.org/10.1039/c3lc51093j.
Sin, A., Chin, K.C., Jamil, M.F., Kostov, Y., Rao, G., Shuler, M.L., 2004. The design and fabrication of three-chamber microscale cell culture analog devices with integrated dissolved oxygen sensors. Biotechnol. Prog. 20, 338–345, http://dx.doi.org/10.1021/bp034077d.
Stewart, J.D., Marchan, R., 2012. Current developments in toxicology. EXCLI J. 11, 692–702.
Struck, R.F., Alberts, D.S., Horne, K., Phillips, J.G., Peng, Y.M., Roe, D.J., 1987. Plasma pharmacokinetics of cyclophosphamide and its cytotoxic metabolites after intravenous versus oral administration in a randomized, crossover trial. Cancer Res. 47, 2723–2726.
Sung, J.H., Kam, C., Shuler, M.L., 2010. A microfluidic device for a pharmacokinetic-pharmacodynamic (PK-PD) model on a chip. Lab Chip 10, 446–455, http://dx.doi.org/10.1039/b917763a.
Sung, J.H., Shuler, M.L., 2009. A micro cell culture analog (microCCA) with 3-D hydrogel culture of multiple cell lines to assess metabolism-dependent cytotoxicity of anti-cancer drugs. Lab Chip 9, 1385–1394, http://dx.doi.org/10.1039/b901377f.
Tan, W., Desai, T.a., 2004. Layer-by-layer microfluidics for biomimetic three-dimensional structures. Biomaterials 25, 1355–1364, http://dx.doi.org/10.1016/j.biomaterials.2003.08.021.
Thoma, C.R., Stroebel, S., Rösch, N., Calpe, B., Krek, W., Kelm, J.M., 2013. A high-throughput-compatible 3D microtissue co-culture system for phenotypic RNAi screening applications. J. Biomol. Screen. 18, 1330–1337, http://dx.doi.org/10.1177/1087057113499071.
Timmins, N.E., Nielsen, L.K., 2007. Generation of multicellular tumor spheroids by the hanging-drop method. Methods Mol. Med. 140, 141–151.
Toh, Y.-C., Lim, T.C., Tai, D., Xiao, G., van Noort, D., Yu, H., 2009. A microfluidic 3D hepatocyte chip for drug toxicity testing. Lab Chip 9, 2026–2035, http://dx.doi.org/10.1039/b900912d.
Torisawa, Y., Takagi, A., Nashimoto, Y., Yasukawa, T., Shiku, H., Matsue, T., 2007. A multicellular spheroid array to realize spheroid formation, culture, and viability assay on a chip. Biomaterials 28, 559–566, http://dx.doi.org/10.1016/j.biomaterials.2006.08.054.
Ullrich, A., Stolz, D.B., Ellis, E.C., Strom, S.C., Michalopoulos, G.K., Hengstler, J.G., Runge, D., 2009. Long term cultures of primary human hepatocytes as an alternative to drug testing in animals. ALTEX 26, 295–302.
Van Midwoud, P.M., Verpoorte, E., Groothuis, G.M.M., 2011. Microfluidic devices for in vitro studies on liver drug metabolism and toxicity. Integr. Biol. (Camb). 3, 509–521, http://dx.doi.org/10.1039/c0ib00119h.
Wagner, I., Materne, E.-M., Brincker, S., Süßbier, U., Frädrich, C., Busek, M., Sonntag, F., Sakharov, D.a., Trushkin, E.V., Tonevitsky, A.G., Lauster, R., Marx, U., 2013. A dynamic multi-organ-chip for long-term cultivation and substance testing proven by 3D human liver and skin tissue co-culture. Lab Chip 13, 3538–3547, http://dx.doi.org/10.1039/c3lc50234a.
Wu, L.Y., Di Carlo, D., Lee, L.P., 2008. Microfluidic self-assembly of tumor spheroids for anticancer drug discovery. Biomed. Microdevices 10, 197–202, http://dx.doi.org/10.1007/s10544-007-9125-8.
Yamada, K.M., Cukierman, E., 2007. Modeling tissue morphogenesis and cancer in 3D. Cell 130, 601–610, http://dx.doi.org/10.1016/j.cell.2007.08.006.
Zhang, C., Zhao, Z., Abdul Rahim, N.A., van Noort, D., Yu, H., 2009. Towards a human-on-chip: culturing multiple cell types on a chip with compartmentalized microenvironments. Lab Chip 9, 3185–3192, http://dx.doi.org/10.1039/b915147h.

Please cite this article in press as: Kim, J.-Y., et al., 3D spherical microtissues and microfluidic technology for multi-tissue experiments and analysis. J. Biotechnol. (2015), http://dx.doi.org/10.1016/j.jbiotec.2015.01.003